

# Chapter 20

## A Geophysical and Remote Sensing-Based Approach for Monitoring Land Subsidence in Saudi Arabia



Abdullah Othman and Karem Abdelmohsen

**Abstract** Groundwater represents the main source of accessible freshwater in Saudi Arabia. Overexploitation of these resources can adversely lead to serious natural hazards in these regions. Understanding the mechanisms and factors causing these hazards whether natural or anthropogenic have become essential to safe people life and sustain the development in such arid regions. Here we applied an integrated approach (field, Interferometric Synthetic Aperture Radar [InSAR], hydrogeology, Geoinformatics) over the northern and central parts of Saudi Arabia to identify the nature, intensity, and spatial distribution of deformational features. The Lower Mega Aquifer System (LMAS) in central and northern Saudi Arabia were used as a test sites. Findings suggest that the natural recharge reduction and excessive groundwater extraction in the LMAS are the major cause of land subsidence and deformation features in the study site. Spatial and temporal correlation of radar and Gravity Recovery and Climate Experiment (GRACE) solutions indicated that sustainable extraction could be attained by reducing the current extraction rates. This approach provides replicable and cost-effective approach for ideal utilization of fossil aquifers in arid lands and for reducing deformation hazards associated with their use. Also suggesting potential areas for sustainable agricultural development that will lead to concrete actions and have an immediate humanitarian/community/environmental benefits.

**Keywords** GRACE: Radar interferometry · InSAR · Fossil aquifers · Land subsidence · Saudi Arabia

---

A. Othman (✉)

Department of Environmental Engineering, Umm Al-Qura University, Makkah, Saudi Arabia  
e-mail: [agothman@uqu.edu.sa](mailto:agothman@uqu.edu.sa)

K. Abdelmohsen

Department of Geological and Environmental Sciences, Western Michigan University,  
Kalamazoo, MI, USA

## 20.1 Introduction

Understanding the factors that causing natural disasters and hazards whether natural or anthropogenic factors have become essential to safe people life and assessing the development in arid and semi-arid regions. Land subsidence can substantially jeopardize human lives and infrastructures. This phenomenon represents a response to the differential subsiding of the ground surface due to the extent reduction of belowground materials by compaction or collapse of subsurface cavities (Ren et al., 1989). Land subsidence a result of volume reduction, either by natural or anthropogenic activities, is typically a slow process happening over nearly large areas. The rates of subsidence have been traditionally measured using ground-based surveying methods (e.g., geodetic leveling and global positioning systems) (Galloway & Burbey, 2011). Yet, the advancement of the Interferometric Synthetic Aperture Radar (InSAR) technologies enabled cost-effective and timely estimations of land subsidence over large-scales (Gabriel et al., 1989). Examples of these applications include; some areas in California and Las Vegas such as Antelope, Santa Clara, and Las Vegas valleys (Galloway et al., 1998; Galloway & Hoffmann, 2007), The Nile Delta in Egypt (Becker & Sultan, 2009; Rateb & Abotalib, 2020) and central Arabia (Othman & Abotalib, 2019). Moreover, (InSAR) technologies have been recently used to detect and quantify sluggish, large property displacements all over the globe (Hooper, 2006; Kampes, 2006), such as technologies enabled cost-effective San Francisco Bay Area (Bürgmann et al., 2006) and central Mexico (Chaussard et al., 2014). The relationship between radar-detected subsidence and related spatial-temporal measurements sheds light on the factors that cause the reported subsidence. (Higgins et al., 2014). These factors usually include groundwater or oil/gas extraction rates, rapid urbanization (Al-Jammaz et al., 2021), decline in groundwater levels, and the distribution of different lithologies. For example, significant subsidence of over 40 mm over 35 days in the oil fields over Lost Hills and Belridge in San Joaquin Valley, California was attributed to immoderate oil production from depths of about 700 m under the ground (Fielding et al., 1998). Subsidence and related deformations such as fissures, sinkholes, and earthquakes, have been reported in many arid and semi-arid regions, where excessive groundwater extraction is a common practice. In Las Vegas Valley, between 1992 to 1997, and by using geodetic and satellites applications such as GPS and InSAR data, deformational features, and land subsidence of up to six centimeters by year were discovered due to intensive pumping of groundwater ( $93 \text{ km}^3/\text{year}$ ) (Bell et al., 2002). Significant land deformation and subsidence were also reported from Mashhad city northern Iran, where InSAR measurements indicated subsidence of  $\sim 28\text{--}30 \text{ cm/y}$  between 2003 and 2005 along the axis of the Mashhad valley. These rates were set on as main factors caused by extensive extraction of the aquifer system as evident by analysis of piezometric records (i.e. 65 m of water table decline since 1960s) (Motagh et al., 2007). Moreover, Earth fissures were reported from the Sarir South agricultural project over the Nubian Sandstone Aquifer System (NSAS) in Libya, where water levels dropped by more than 6 meters leading to compaction of fine-grained

sediments within the aquifer materials and development of earth fissures (El Baruni, 1994). In the same context, using GPS data from two stations (period: 2006 to 2009), subsidence rates of up to 10 cm per a year were reported from the Quetta Valley in Pakistan, where subsidence was also attributed to excessive groundwater abstraction to support progressive population growth (1975: 260,000; 2010: 1.2 million) (Khan et al., 2013). Groundwater-extraction-induced deformation was reported for both confined and unconfined aquifers (Galloway et al., 1998; Othman & Abotalib, 2019). The reported deformation was either uniform and extend over large areas, or differential, causing earth fissures, damage in buildings and infrastructures (Burbey, 2002) and might involve horizontal displacement in addition to the vertical component (Burbey, 2001; Galloway & Burbey, 2011).

The largest number of subsidence cases were documented in arid lands, where precipitation was minimal, limited or no surface water resources were available, intensive irrigation programs were implemented mainly on groundwater as a source for freshwater (Maliva & Missimer, 2012) such as the Saharan-Arabian desert belt. Aquifers in the Saharan-Arabian deserts are fossil aquifers that were recharged mainly during the Quaternary wet climatic periods (Abotalib et al., 2016, 2019a). Currently, they receive only limited local recharge, which is way lower than the annual abstraction (Sultan et al., 2014). Examples of these aquifers include the Mega Aquifer System (MAS) in Saudi Arabia (Hoetzel et al., 1978; Sultan et al., 2014; Abotalib et al., 2019b), the Nubian Aquifer System in northeastern Africa (Abdelmohsen et al., 2020; Mohamed et al., 2017), the North-Western Sahara Aquifer System in northwestern Africa, and the Great Artesian Basin in Australia (Taylor et al., 2013).

Overstimulated exploitation of non-renewable groundwater in such regions, and for certain fossil aquifers, will be expected to cause artesian head downturn, high extensional stresses, and other problems.

In this study, we are investigating on the LMAS of Saudi Arabia, one of the world's largest fossil aquifer systems, examine comparable cases elsewhere, and note the similarity with our results from the LMAS to those published from similar areas around the world. The Mega Aquifer System (MAS) (surface area: ~2 million km<sup>2</sup>) spans the Arabian Peninsula's Arabian Shelf in Saudi Arabia, United Arab Emirates (UAE), Qatar, Yemen, Oman, Jordan and Kuwait. The aquifer currently is the major water resource for mega-agricultural projects and within these reclaimed areas, several ground deformations and subsidence features were reported. Examples of these areas are the Al-Yutamah valley, Tabah village, and Najran valley (Roobol et al., 1985; Vincent, 2008; Youssef et al., 2014).

The government of Saudi Arabia started in the mid-eighties an ambitious agricultural development program in central Arabia (e.g. Al-Qassim and Ha'il regions central Saudi Arabia), which led to a raise in groundwater extraction ( $1.9 \times 10^9$  m<sup>3</sup>/year in 1984 to  $4.4 \times 10^9$  m<sup>3</sup>/year in 2004) and cultivated lands (from  $213 \times 10^3$  hectares in 1984 to  $316 \times 10^3$  hectares in 2004). Likewise, widespread agricultural projects were employed in northern Saudi Arabia (e.g. As-Sirhan valley northern Saudi Arabia) leading to a raise in groundwater extraction from  $0.095 \times 10^9$  m<sup>3</sup>/year

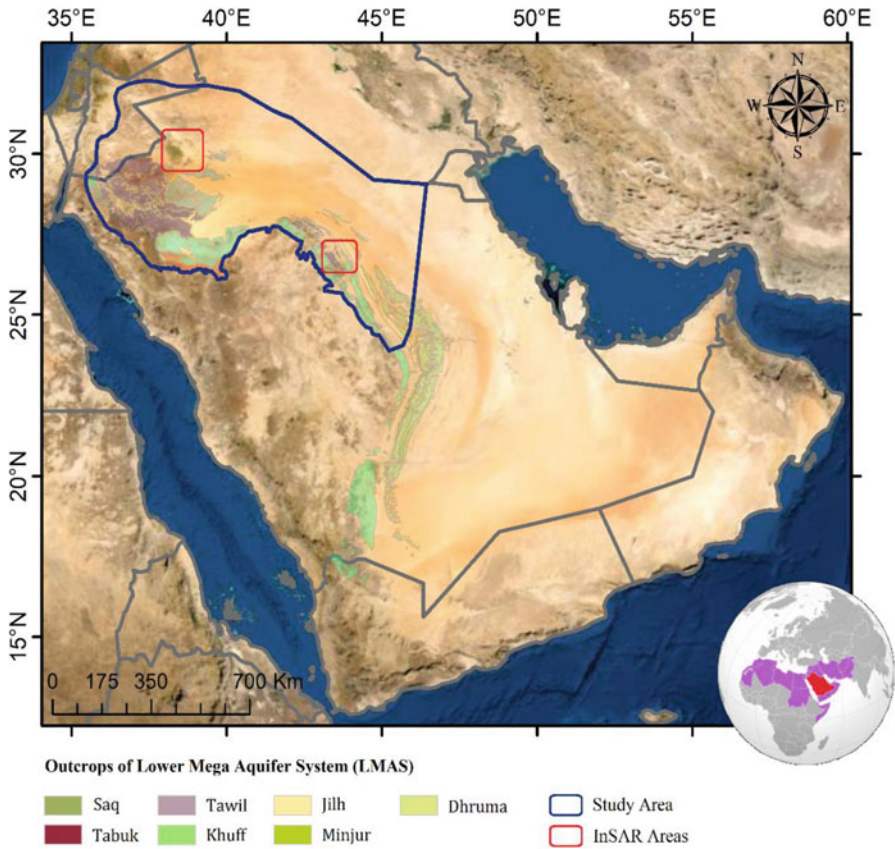


**Fig. 20.1** Location map of the regional study area and the investigated InSAR areas over Wadi As-Sirhan Basin and Al-Qassim Region. The boundaries and outcrops of the Lower Miga Aquifer System

to  $2 \times 10^9 \text{ m}^3/\text{year}$ , the cultivated areas have grown from  $14 \times 10^3$  hectare in 1984 to  $164 \times 10^3$  hectare in 2004 (MOAW, 1984, 2004; Abunayyan and BRGM, 2008).

Our integrated study includes a regional investigation over LMAS in northern and central parts of the KinSaudi Arabia and a local investigation over the Wadi As-Sirhan Basin (WASB) and Al-Qassim Region (Fig. 20.1). The regional investigation implemented field observations to examine deformational land features and applying spatial correlation for features with other relevant datasets in term of causal effects.

## 20.2 Geology and Hydrogeology of the Study Area

The Arabian Shield's basement complex crops out along Red Sea margins, creating the Red Sea mountain range (Red Sea Hills) (Fig. 20.2). Successions of Phanerozoic sedimentary overlie the basement complex unconformably, with east-dipping and approaching thicknesses of ten kilometers near the Arabian Gulf (Powers et al., 1966; Lloyd & Pim, 1990; Konert et al., 2001; Margat, 2007). The Red Sea mountains outcrops are younger to the eastward of the Gulf (Quaternary age) and older to the westward (Cambrian age) (Fig. 20.2). The Red Sea rifting exposed the basement complex and the overlying Phanerozoic formation, which facilitates aquifer recharge within the surface exposures of these formations. The Red Sea opening rejuvenated many of the Proterozoic NW-trending Najd fault systems that affect the crystalline rocks of the Arabian Shield (Fairer, 1983; Morsy & Othman, 2020). The fault rejuvenation was dip-slip (e.g. normal faults and grabens) in response to the extensional events associated with Red Sea rifting during the Oligo-Miocene time (Kellogg & Reynolds, 1983; Giannerini et al., 1988). These faults are represented by the Kahf fault system in northern and central Saudi Arabia

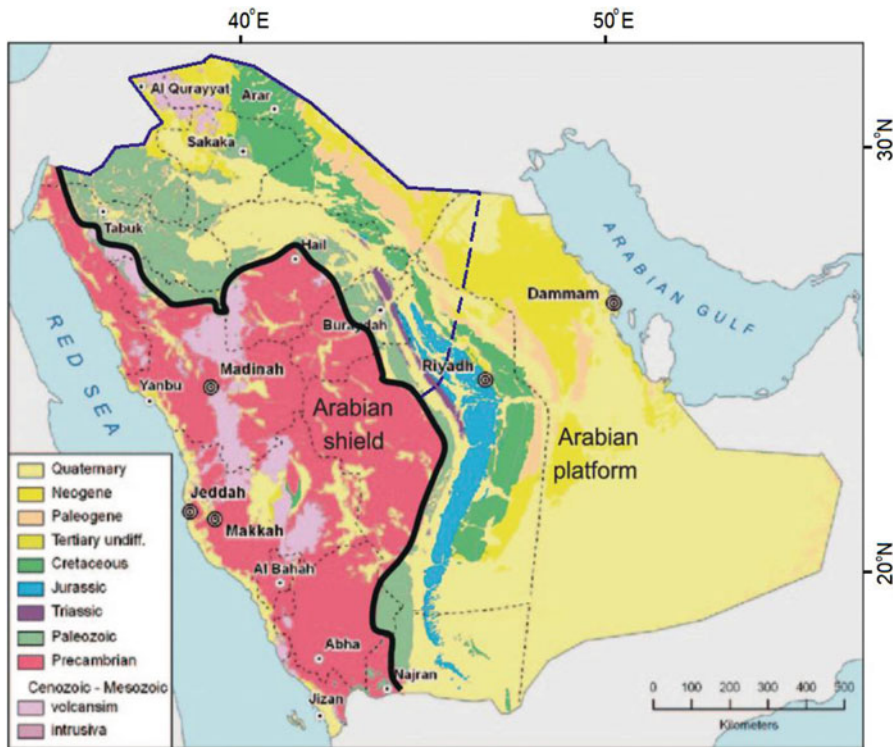


Fig. 20.2 Regional geological map of Saudi Arabia. (After Powers et al., 1966)

(Othman et al., 2018). Similar observations of dip-slip displacement on Najd faults were also reported in the Egyptian side of the shield (Sultan et al., 2011).

Phanerozoic sections contain one of the largest fossil aquifers in the world which formed from sandstone and limestone sequences (Figs. 20.1 and 20.2). The LMAS was primarily recharged during previous wet climatic conditions, but it is still receiving a modern recharge at the moment, especially in southwest Saudi Arabia, where AAP rates of up to 800 mm/y have been recorded (Alharbi et al., 2014). Groundwater Cl-36 ages attained close to 1 million years from some aquifers in the southeastern part of Saudi Arabia (Sultan et al., 2019). Those previous wet climatic conditions are completely different from current arid conditions with an average annual precipitation of 100 mm/y and minimal surface-water resources over Saudi Arabia (Barthélemy et al., 2007).

The main aquifer units within the MAS include formations of Paleozoic sandstone, Mesozoic-Cenozoic carbonates, Paleocene, and Neogene sedimentary formations (Wagner, 2011). The MAS geological have been split into two major groups separated by the anhydrite layer (Hith formation) (Othman et al., 2018). The topmost is the Upper Mega Aquifer System (UMAS), including Damman, Rus, Umm Er Radhuma, Aruma, Wasia, Biyadh formations. Then Lower Mega Aquifer System (LMAS), which contains Dhurma, Minjur, Tawil, Tabuk, Wajid, and Saq formations. The area of MAS is  $\sim 236.3 \times 10^4 \text{ km}^2$ , respectively, respectively.

## 20.3 Methodology

We briefly describe the technical approaches applied in this study to monitor the land deformation over Saudi Arabia using (1) Field observations and land deformation database, (2) TWS and GWS extracted from GRACE temporal monthly solutions, (3) Radar Interferometric data and (4) precipitation extracted from Tropical Rainfall Measuring Mission (TRMM) data. The spatial and temporal integration of these data sets with other relevant data sets (geologic, geochemical, remote sensing) provides more evidences of the factors controlling the reported deformational features (e.g. sinkholes, fissures, and subsidence) announced in the arid environmental lands over the fossil aquifers.

### 20.3.1 Gravity Recovery and Climate Experiment (GRACE) Data

GRACE is a satellite mission launched in 2002 by the German Aerospace Center (DLR) and National Aeronautics and Space Administration (NASA) for the temporal global variations measurements in the Earth's gravitational field (Tapley et al., 2004) that represents the temporal variation in the TWS (Wouters et al., 2014;

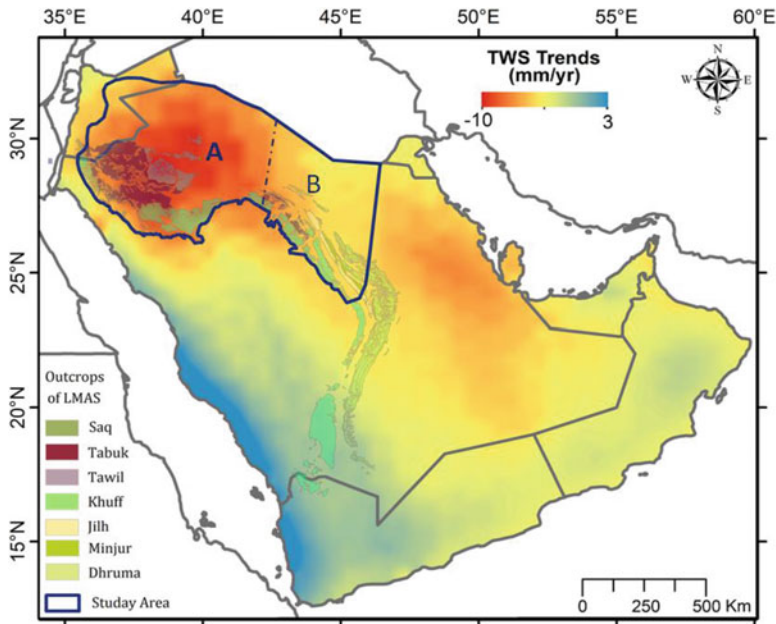


**Fig. 20.3** Secular trend (mm/y) for GRACE-derived TWS for the Arabian Peninsula extracted from temporal (04/2002–03/2016) CSR 1° × 1° Mascon solutions showing high TWS depletion rates over the study areas

Ahmed et al., 2016; Mohamed et al., 2017; Ahmed & Abdelmohsen, 2018; Sultan et al., 2019; Abdelmohsen et al., 2019, 2020). TWS refers to the vertically integrated water storage measurement that includes groundwater, soil moisture storage, surface water storage, snow water storage, and canopy water storage (Strassberg et al., 2007; Abdelmalik & Abdelmohsen, 2019).

Release (05; RL05), with a spatial resolution of 0.5° × 0.5°, temporal monthly constrain solutions (mascon; Save et al., 2016) covering the investigated time period (4/2002 to 6/2016) were utilized to estimate the long-term components of TWS changes over the lower MAS and the WASB. The mascon solutions were provided by Center for Space Research (CSR) at the University of Texas (Save et al., 2016). The mascon solution doesn't require any post processing, analysis, filtering, or scaling factors (Save et al., 2016).

The long term trend TWS component was extracted by continuously fitting a linear regression function (Fig. 20.3) and the trend uncertainty was calculated using an approach described in Scanlon et al. (2016). The change in groundwater storage was calculated using a common equation of water mass:

$$\Delta GWS = \Delta TWS - \Delta SMS \tag{20.1}$$

Where  $\Delta GWS$  and  $\Delta SMS$  represent the variation in groundwater storage and soil moisture storage, respectively. Global Land Data Assimilation System (GLDAS) model was utilized to derive SMS. land surface modeling system developed by NASA as a simulation model for hydrologic and climatic variables (Rodell et al., 2004). Four GLDAS models to estimate the soil moisture: Community Land Model [CLM], Noah, and MOSAIC, Variable Infiltration Capacity [VIC] were used to represent the soil moisture over the study area (Rodell et al., 2004; Dai et al., 2003). The uncertainty ( $\sigma_{SM}$ ) were calculated from the standard deviation (STD) of the trends from the GLDAS four simulations. The trend uncertainty in GWS ( $\sigma_{GWS}$ ) was calculated using standard error propagation equations:

$$\sigma_{GWS} = \sqrt{(\sigma_{TWS})^2 + (\sigma_{SM})^2} \quad (20.2)$$

### 20.3.2 Radar Interferometric Data (Persistent Scatterer Interferometry)

Twenty-nine descending scenes from the European Remote Sensing ENVISAT satellite were implemented. Twenty-two of those scenes covered the Wadi As-Sirhan Basin (Tabarjal and Busayta area, tracks: 221, 351 and 493) and the remaining eight scenes were acquired over Al-Qassim area (Track: 49 and 278). The investigated period for the first set was from 2003 to 2012, while the second set covered the period between 2003 and 2005. The spatial baseline ranged from 15 to 855 m concerning the master scenes. The maximum temporal baseline was 1351 days for both investigated areas, and the ranges of permanent scatterers' density from 10 to 251,351 days for both investigated areas, and the ranges of permanent scatterers' density from 10 to 25 persistent scatterers/km<sup>2</sup> with a coherence threshold value of 0.5 and an amplitude dispersion value of 0.4.

Persistent Scatterer Interferometry (PSI) techniques has been applied (Hooper et al., 2004, 2007) to examine the spatial variations in subsidence rates across the two sites on the Northern and southern parts of the study area (LMAS) (Fig. 20.1). The PSI technique restrict the unwrapping phase and analysis to coherent pixels, containing individual scatterers and remaining stable over the investigated period. Buildings, rock formations, rocks, houses, utility poles, and well platforms were classified as persistent scatterers in the study region using the Stanford Approach for Permanent Scatterers (StaMPS) algorithm (Hooper et al., 2007, 2012). The interferometric was processed using the StaMPS process (Hooper et al., 2004). The accurate orbit information was provided from the Delft Institute for Earth-Oriented Space Research (Scharroo & Visser, 1998).



### 20.3.3 Landsat Images

Multi-temporal Landsat (5, 7, and 8) images (path 172 and row 39) were been acquired for the following dates (February 1987, 1991, and 2000, March 2003, January 2014, and February 2017) then were analyzed to monitor the development of cultivated lands throughout the past three decades (1987 to 2017). Temporal changes in the agricultural developments areas were estimated using the NDVI (Normalized Difference Vegetation Index). Using the reflectance values from the near-infrared and red bands, an NDVI value was estimated using standard model and process (Rouse et al., 1974):

$$\text{NDVI} = (\text{near infrared} - \text{red}) / (\text{near infrared} + \text{red}). \quad (20.3)$$

It is a positive relationship between the values of NDVI and density of vegetation. The cultivated land areas were extracted from the Landsat imagery using a threshold NDVI value of 0.3; visual comparisons with Google Earth images validated the threshold value.

## 20.4 Discussion and Findings

Our analysis of the land satellite images and GRACE solutions over the largest aquifer systems in Saudi Arabia revealed that land subsidence features can be targeted excessive extraction of groundwater. In the next parts, we going to describe and explain our findings over the selected areas in relation and relevant deformation factors.

### 20.4.1 The Lower Mega Aquifer System

The excessive groundwater abstraction of the LMAS and unsustainable utilization of the aquifers was reflected in TWS from GRACE solutions. Depletions in TWS and GWS derived from GRACE over LMAS (areas: A and B) were observed. The spatial and temporal changes in TWS anomaly over Saudi Arabia and entire the Arabian platform is shown in Fig. 20.3. Positive TWS trends indicate an increase in water mass with time and vice versa in the areas of the negative TWS trends. Figure 20.3 depicts that the study area over LMAS and WASB (Fig. 20.3 area A) are experiencing a significant decrease in TWS trend (red and orange), compared to the southern areas (Fig. 20.3 area B (Al-Qassim Region)) that extend from lower depletion (yellow and orange) to near-steady statuses (blue) over the Red Sea seaboard plain. Figure 20.3 shows the temporal differences in GRACE-derived TWS, and the secular trend over the WASB in LMAS (area A) ( $-8.7 \pm 1.1$  mm/year;

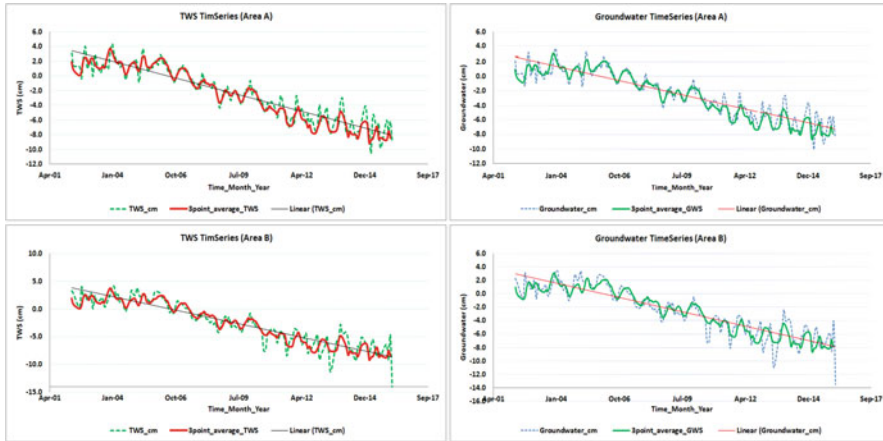


**Fig. 20.4** Time series and secular trends for TWS and GWS over the area A and area B in the regional study area (LMAS)

$-3.1 \pm 0.3 \text{ km}^3/\text{year}$ ) and Al-Qassim Region (area B) ( $-9.5 \pm 1.4 \text{ mm}/\text{year}$ :  $-1.7 \pm 0.2 \text{ km}^3/\text{year}$ ). Using TWS derived from GRACE solutions combined with soil moisture derived from GLDAS applied to Eq. 20.1, GWS time series for both WASB and LMAS were derived (Fig. 20.4).

The observed TWS and GWS seasonal periodical cycle were controlled mainly by groundwater abstraction. Temperatures in summers (June–August) are high (range:  $28^\circ$  to  $37^\circ \text{C}$ ), compared to winter season temperatures which range between ( $6^\circ$  to  $19^\circ \text{C}$ ), and the rates of evaporation is between 25 to 28 mm/day in the summers season and as low as 0.4 mm/day in the winter seasons (Alsharhan et al., 2001). As a result, agricultural activities and groundwater abstraction got lower during the winter season (December–February) and decline in the summer seasons. Excessive abstraction in the winter season caused water-level declines, and surface land subsidence and the replenishment (gaining mass) during the summer season by infiltration and groundwater flow. Since there is a losing mass rate of  $-4.2 \pm 0.7 \text{ km}^3/\text{year}$  in GWS over the study basin, the extracted groundwater does not fully compensated.

The fissures near the boundaries of the subsidence bowls surrounding Busayta area in WASB and in the southeastern part of Al-Qassim area (Fig. 20.5A and B) were most probably caused by curving beam transforming around the area of deformation, the regions have experienced high lateral extension (Bell et al., 2002; Othman et al., 2018). Fissures also can result from the lateral (horizontal) forces linked with sediment compaction or horizontal pressures caused by extraction; all of these mechanisms produce lateral (horizontal) strain extended along the weakness planes (Helm, 1994). This mechanism could have caused Earth fissures that are located proximal to faults. The fissures close to the Kahf fault system in Area A and B in Figs. 20.5 and 20.6 are good examples of this deformation mechanism.

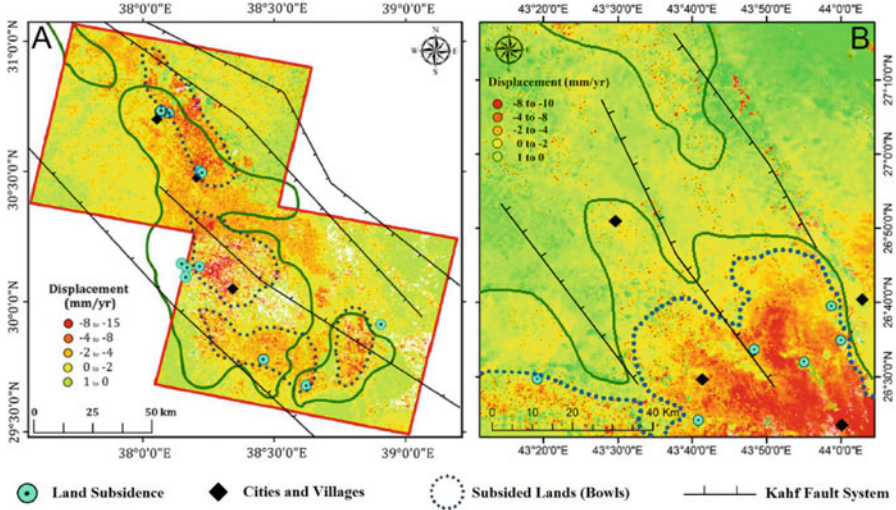


**Fig. 20.5** “A” PSI results over Wadi As-Sirhan (Busayta and Tabarjal areas) “B” and the Al-Qassim region. The distribution of the major faults are also depicted with black lines. (Modified after Wallace et al., 2000)

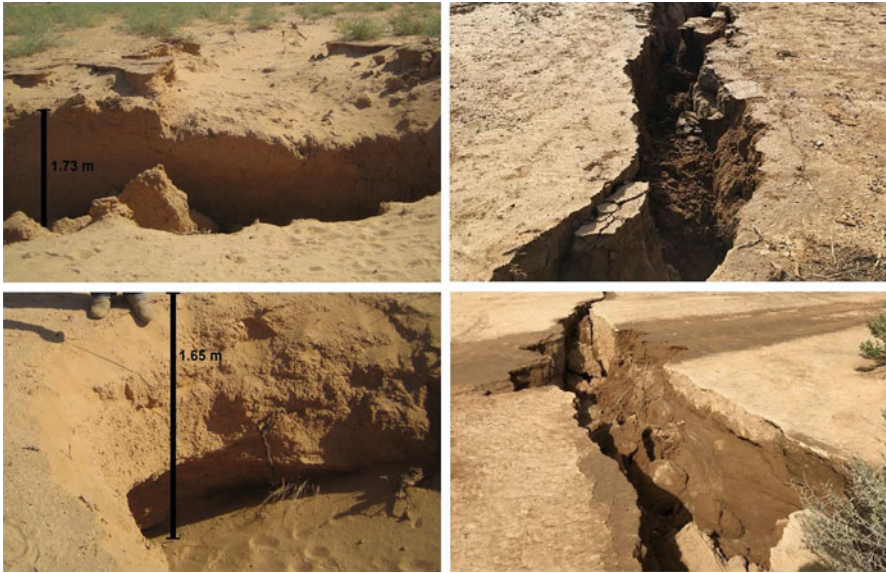


**Fig. 20.6** Field photos showing land fissures and sinkholes proximal to the land subsidence in the study areas

Our research findings are consistent with land subsidence phenomena associated with aquifers depletion which reported from numerous places around the world (e.g., Poland, 1960; Galloway et al., 1998; Hoffmann et al., 2001; Burbey, 2002; Bell et al., 2002; Christiansen et al., 2007; Assumpção et al., 2010; Galloway & Burbey, 2011; González et al., 2012; Avouac, 2012; Martínez et al., 2013; Amos et al., 2014). The detected subsided lands in these areas were attributed to increased adequate pressure that causes layer compaction and land deformation and subsidence (Donaldson et al., 1995). The effective stress balanced the downward stress effect due to the overload the overlying rock, water effective stress and pore pressure balanced the downward stress from the overlying rock and water. The changes in groundwater extraction-induced stresses trigger earthquakes and land deformations that would have occurred later when natural stress is accumulated (Avouac, 2012).

The illustrated land subsidence in the northern central part of the Kingdom of Saudi Arabia has a similar patter to other global aquifer systems in terms of theresponse to overexploitation of groundwater and the significant associated draw-down of water table such as in the Mojave Desert, California (Galloway et al., 1998), central and northeast Iran (Motagh et al., 2008) and in North China Plain (Guo et al., 2015). Such aquifers are expecting to show near-steady GWS secular trends, and stable velocity (0 radar averaged velocity) (Chew & Small, 2014). The case from LMAS is different because the fossil aquifer was primarily recharged in previous wet climatic periods yet still receives a small amount of recharge (Sultan et al., 2008). LMAS is not in near-stable state condition according to two observations. Which groundwater abstraction from the LMAS was not compensated for by replenishment; (1) the depletion in TWS ( $-4.8 \pm 0.7 \text{ km}^3/\text{year}$ ) and GWS ( $-4.2 \pm 0.7 \text{ km}^3/\text{year}$ ) over the investigated period (Figs. 20.3 and 20.4) the radar interferometric technique studies over WASB and Al-Qassim Regions produce deformation rates of  $-4$  to  $-15 \text{ mm/year}$  (Fig. 20.5A and B). The regional deformation in the study basin is attributed mainly to a rise in effective stress that accelerate compaction and land subsidence (Fig. 20.5). The balance between the downward stress from the overload of the upper layers and the upward buoyancy force by the groundwater is challenged by the overexploitation from the Saq aquifer, where the rate of annual groundwater withdrawal exceeds 100 times the rate of annual recharge (et Minières, B.D.R.G., 2006). This overexploitation reduce pore pressure in the aquifer layers causing expand effective stress, which causes compaction and land subsidence in this location (Donaldson et al., 1995).

The MAS in the upper part Saudi Arabia shows the vertical hydrological connection between the aquifer layers due to the structural control and preferred pathways for groundwater flows (e.g. Kahf fault system) and the geological incompatibility associated with differential deposition of aquifer layers (Othman et al., 2018) (McGillivray & Hussein, 1992), (et Minières, B.D.R.G., 2006). The vertical connection between the deep gaseous-rich Saq aquifer (e.g. H<sub>2</sub>S and CO<sub>2</sub>; Kalin et al., 2001) and the upper Paleozoic and Triassic hyrologic layers leads to enhanced evaporation and leakaes from Saq aquifer and dissolution of limestones formations and forming the karst topography during the wet climatic periods and associated elevation of the groundwater level (Abotalib et al., 2016). These karst remain

mechanically stable under different climatic conditions until water table drawdown, which causes instability over the pre-existing subsurface cavities. This kind of mechanism was reported as the primary mechanism of formation of falling features in the Arabian Peninsula to the eastern region (Abotalib et al., 2019b). It can illustrate the formation of local land fall features in the region of study. More evidence of support the latest mentioned mechanism is supported by the field observation/description of sinkholes northern of Buriyadah City in Al-Qassim Region (Youssef et al., 2016). The abovementioned mechanisms, which induced by groundwater dynamics, however controlling the study basin doesn't rule out the influence of the geotechnical properties of the lithological units on the surface deformation in the study basin. The illustrated features of cracks and fissures in Fig. 20.6 might be affected by the existence of near surface approximately thick layer of up to 15 m with high plastic clay beds, causes upward rupture structure when sub-ground layers damping from close agricultural activities extends these beds (Al Fouzan & Dafalla, 2013). Consequently, the mixture of dissolution and subsequent sagging and landfall of the upper layers due to the drop down of groundwater level and the existence of high plastic clay layers with the hydrological and geological factors and the availability of suitable geological and hydrological conditions (e.g. loss of buoyancy) can cause the reported regional and local landfall features in the study basin.

## 20.5 Summary and Implications

The LMAS, one of the highly hydrologic conductive aquifers in the Middle East and North Africa, represents a significant source of groundwater abstraction for irrigation in the upper part of Saudi Arabia. Mainly, this sandstone fossil aquifer of the Paleozoic age has been inordinately mined throughout the past 50 years, causing regional groundwater table dropdown of up to 150 m. The subsidence locations inferred from the InSAR processing maps strongly correlate with GRACE-derived TWS results suggesting that the subsidence can result from excessive groundwater extraction resources. The rapid increase in the cultivated lands between 1987 and 2012 supports this phenomenon (Fig. 20.7) that continues to our present time. Findings from the present study support that excessive fossil groundwater abstraction is critical for forming land subsidence, collapse features, and earth fissures in the study areas. However, the formation of such features might be associated with other factors. The studied approach could provide a simplified and cost-effective method to assess the surface land deformations and landscape associated with anthropogenic and/or natural induced variations in the groundwater tables under arid/semi-arid to hyper-arid conditions.

**Acknowledgments** The authors are grateful for Umm Al-Qura University, the University of Texas at Austin (Space Research Center), European Space Agency, Ministry of Environment, Water and Agriculture, and Saudi Geological Survey for their data, field, and logistical support.

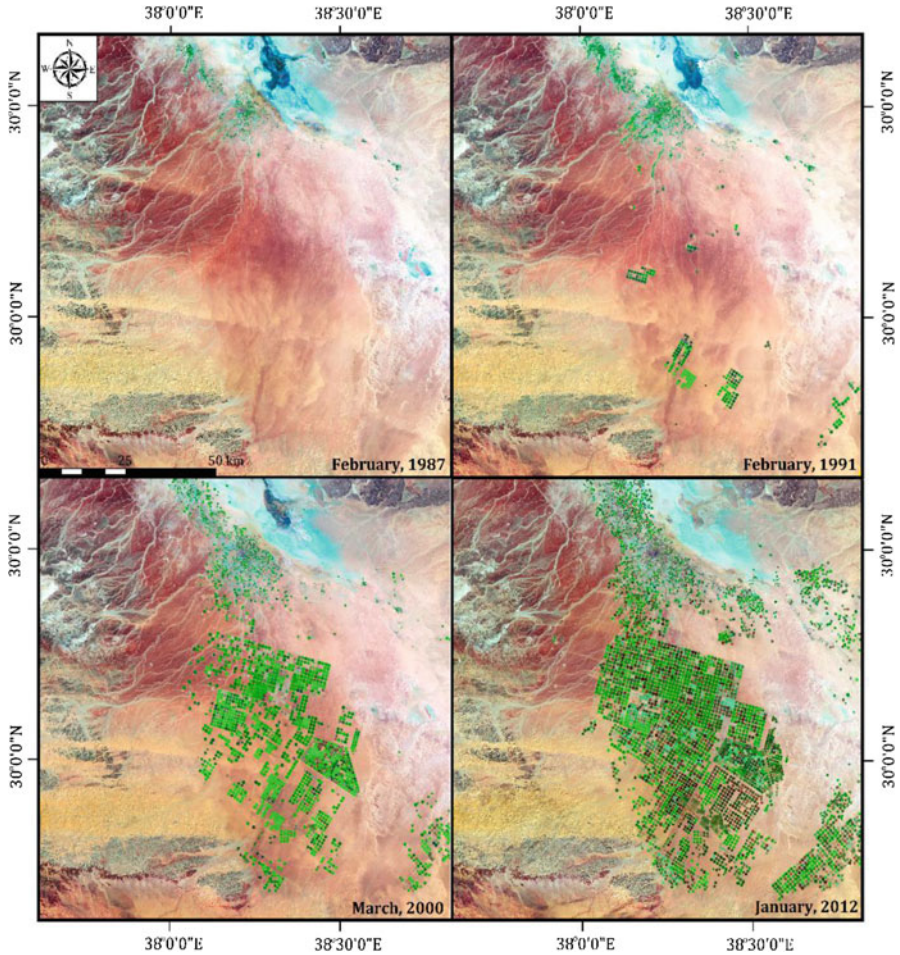


**Fig. 20.7** Time series for Landsat 5, 7 and 8 scenes acquired (February 1987, February 1991, February 2000, January 2012) over Busayta area in Wadi As-Sirhan Basin (WASB). (Source: Earth Resources Observation and Science (EROS) Center)

## References

- Abdelmalik, K. W., & Abdelmohsen, K. (2019). GRACE and TRMM mission: The role of remote sensing techniques for monitoring spatio-temporal change in total water mass, Nile basin. *Journal of African Earth Sciences*, 160. <https://doi.org/10.1016/j.jafrearsci.2019.103596>
- Abdelmohsen, K., Sultan, M., Ahmed, M., Save, H., Elkaliouby, B., Emil, M., Yan, E., Abotalib, A. Z., Krishnamurthy, R. V., & Abdelmalik, K. (2019). Response of deep aquifers to climate variability. *Science of the Total Environment*, 677, 530–544. <https://doi.org/10.1016/j.scitotenv.2019.04.316>

- Abdelmohsen, K., Sultan, M., Save, H., & Abotalib, Z. A. (2020). What can the GRACE seasonal cycle tell us about lake-aquifer interactions? *Earth-Science Reviews*. <https://doi.org/10.1016/j.earscirev.2020.103392>
- Abotalib, A. Z., Sultan, M., & Elkadiri, R. (2016). Groundwater processes in Saharan Africa: Implications for landscape evolution in arid environments. *Earth-Science Reviews*, 156, 108–136.
- Abotalib, A. Z., Sultan, M., Jimenez, G., Crossey, L., Karlstrom, K., Forman, S., ... Polyak, V. (2019a). Complexity of Saharan paleoclimate reconstruction and implications for modern human migration. *Earth and Planetary Science Letters*, 508, 74–84.
- Abotalib, A. Z., Heggy, E., Scabbia, G., & Mazzoni, A. (2019b). Groundwater dynamics in fossil fractured carbonate aquifers in Eastern Arabian Peninsula: A preliminary investigation. *Journal of Hydrology*, 571, 460–470.
- Abunayyan BRGM. (2008). *Investigations for updating the groundwater mathematical model(s) of the Saq overlying aquifers*. Ministry of Water and Electricity.
- Ahmed, M., & Abdelmohsen, K. (2018). Quantifying modern recharge and depletion rates of the Nubian Aquifer in Egypt. *Surveys in Geophysics*, 39(4), 729–751. <https://doi.org/10.1007/s10712-018-9465-3>
- Ahmed, M., Sultan, M., Yan, E., & Wahr, J. (2016). Assessing and improving land surface model outputs over Africa using GRACE, field, and remote sensing data. *Surveys in Geophysics*, 37, 529–556.
- Al Fouzan, F., & Dafalla, M. A. (2013). Study of cracks and fissures phenomenon in Central Saudi Arabia by applying geotechnical techniques. *Arabian Journal of Geosciences*, 7, 1157–1164.
- Alharbi, T., Sultan, M., Sefry, S., et al. (2014). An assessment of landslide susceptibility in the Faifa area, Saudi Arabia, using remote sensing and GIS techniques. *Natural Hazards and Earth System Sciences*, 14, 1553–1564.
- Al-Jammaz, A., Sultan, M., Izadi, M., Abotalib, A. Z., Elhebiry, M. S., Emil, M. K., Abdelmohsen, K., Saleh, M., & Becker, R. (2021). Land subsidence induced by rapid urbanization in arid environments: A remote sensing-based investigation. *Remote Sensing*, 13, 1109. <https://doi.org/10.3390/rs13061109>
- Alsharhan, A., Rizk, Z., Nairn, A. E., Bakhit, D., et al. (2001). *Physical geography of the Arabian peninsula, hydrogeology of an arid region: The Arabian gulf and adjoining areas* (pp. 7–42). Elsevier.
- Amos, C. B., Audet, P., Hammond, W. C., et al. (2014). Uplift and seismicity driven by groundwater depletion in Central California. *Nature*, 509(7501), 483–486.
- Assumpção, M., Yamabe, T. H., Barbosa, J. R., et al. (2010). Seismic activity triggered by water wells in the Paraná Basin, Brazil. *Water Resources Research*, 46(7), W07527.
- Avouac, J. P. (2012). Earthquakes: Human-induced shaking. *Nature Geoscience*, 5(11), 763–764.
- Barthélemy, Y., Béon, O., Le Nindre, Y., et al. (2007). *Modelling of the Saq aquifer system (Saudi Arabia). Aquifer systems management: Darcy's legacy in a world of impending water shortage* (pp. 175–190). Taylor & Francis.
- Becker, R. H., & Sultan, M. (2009). Land subsidence in the Nile delta: Inferences from radar interferometry. *The Holocene*, 19, 949–954.
- Bell, J. W., Amelung, F., Ramelli, A. R., & Blewitt, G. (2002). Land subsidence in Las Vegas, Nevada, 1935–2000: New geodetic data show evolution, revised spatial patterns, and reduced rates. *Environmental & Engineering Geoscience*, 8(3), 155–174.
- Burbey, T. J. (2001). Storage coefficient revisited: Is purely vertical strain a good assumption? *Groundwater*, 39, 458–464.
- Burbey, T. J. (2002). The influence of faults in basin-fill deposits on land subsidence, Las Vegas valley, Nevada, USA. *Hydrogeology Journal*, 10, 525–538.
- Bürgmann, R., Hillel, G., Ferretti, A., & Novali, F. (2006). Resolving vertical tectonics in the San Francisco Bay area from permanent scatterer InSAR and GPS analysis. *Geology*, 34, 221–224.
- Chaussard, E., Wdowinski, S., Cabral-Cano, E., & Amelung, F. (2014). Land subsidence in Central Mexico detected by ALOS InSAR time-series. *Remote Sensing of Environment*, 140, 94–106.

- Chew, C. C., & Small, E. E. (2014). Terrestrial water storage response to the 2012 drought estimated from GPS vertical position anomalies. *Geophysical Research Letters*, *41*, 6145–6151.
- Christiansen, L. B., Hurwitz, S., & Ingebritsen, S. E. (2007). Annual modulation of seismicity along the San Andreas Fault near Parkfield, CA. *Geophysical Research Letters*, *34*(4), L04306.
- Dai, Y., Zeng, X., Dickinson, R. E., Baker, I., et al. (2003). The common land model. *Bulletin of the American Meteorological Society*, *84*, 1013–1023.
- Donaldson, E. C., Chilingarian, G. V., & Yen, T. F. (1995). Stresses in sediments (Chapter 3). In *Subsidence due to fluid Withdrawal* (pp. 165–190). Elsevier.
- El Baruni, S. (1994). Earth fissures caused by groundwater withdrawal in Sarir South agricultural project area, Libya. *Applied Hydrogeology*, *2*, 45–52.
- Fairer, G. M. (1983). Reconnaissance geology of the Ishash Quadrangle, Sheet 26/39C, Kingdom of Saudi Arabia, U. S. Geological Survey, No. 83–821, Reston, Virginia, Saudi Arabia.
- Fielding, E. J., Blom, R. G., & Goldstein, R. M. (1998). Rapid subsidence over oil fields measured by SAR interferometry. *Geophysical Research Letters*, *25*, 3215–3218.
- Gabriel, A. K., Goldstein, R. M., & Zebker, H. A. (1989). Mapping small elevation changes over large areas: Differential radar interferometry. *Journal of Geophysical Research: Solid Earth*, *94*, 9183–9191.
- Galloway, D. L., & Burbey, T. J. (2011). Review: Regional land subsidence accompanying groundwater extraction. *Hydrogeology Journal*, *19*, 1459–1486.
- Galloway, D. L., & Hoffmann, J. (2007). The application of satellite differential SAR interferometry-derived ground displacements in hydrogeology. *Hydrogeology Journal*, *15*, 133–154.
- Galloway, D. L., Hudnut, K. W., Ingebritsen, S., et al. (1998). Detection of aquifer system compaction and land subsidence using interferometric synthetic aperture radar, Antelope Valley, Mojave Desert, California. *Water Resources Research*, *34*, 2573–2585.
- Giannerini, G., don Campre, R., Feraud, G., & Zakhem, B. A. (1988). Deformations intraplaques et volcanisme associe; exemple de la bordure NW de la plaque Arabique au Cenozoique. *Bulletin De La Société Géologique De France*, *4*(6), 937–947.
- González, P. J., Tiampo, K. F., & Palano, M. (2012). The 2011 Lorca earthquake slip distribution controlled by groundwater crustal unloading. *Nature Geoscience*, *5*(11), 821–825.
- Guo, H. P., Zhang, Z. C., Cheng, G. M., Li, W. P., Li, T. F., & Jiao, J. J. (2015). Groundwater-derived land subsidence in the North China plain. *Environment and Earth Science*, *74*(2), 1415–1427.
- Helm, D. C. (1994). Hydraulic forces that play a role in generating fissures at depth. *Bulletin of the Association of Engineering Geologists*, *31*(3), 293–304.
- Higgins, S. A., Overeem, I., Steckler, M. S., Syvitski, J. P., Seeber, L., & Akhter, S. H. (2014). InSAR measurements of compaction and subsidence in the Ganges-Brahmaputra delta, Bangladesh. *Journal of Geophysical Research: Earth Surface*, *119*, 1768–1781.
- Hoetzel, H., Felber, H., & Zoetl, J. (1978). *The quaternary development of the upper part of Wadi Ar-Rimah (Saudi Arabia)*. *Quaternary period in Saudi Arabia* (pp. 173–182). Springer.
- Hoffmann, J., Zebker, H. A., Galloway, D. L., & Amelung, F. (2001). Seasonal subsidence and rebound in Las Vegas Valley, Nevada, observed by synthetic aperture radar interferometry. *Water Resources Research*, *37*(6), 1551–1566.
- Hooper A J (2006) Persistent scatter radar interferometry for crustal deformation studies and modeling of volcanic deformation. , Stanford University.
- Hooper, A., Zebker, H., Segall, P., & Kampes, B. (2004). A new method for measuring deformation on volcanoes and other natural terrains using InSAR persistent scatterers. *Geophysical Research Letters*, *31*, L23611.
- Hooper, A., Segall, P., & Zebker, H. (2007). Persistent scatterer interferometric synthetic aperture radar for crustal deformation analysis, with application to Volcán Alcedo, Galápagos. *Journal of Geophysical Research: Solid Earth*, *112*, B07407.
- Hooper, A., Bekaert, D., Spaans, K., & Ankan, M. (2012). Recent advances in SAR interferometry time series analysis for measuring crustal deformation. *Tectonophysics*, *514*, 1–13.



- Kalin, R. M., Elliot, T., Suba, A., Katbeh, H., Rimawi, O., IA, A. L.-H., & Aleissa, K. (2001). *Sustainability of groundwater resources in water-scarce regions: From micro-to macro-scales* (Reports submitted to Natural Resources & Environment Research Institute) (p. 56p). King Abdulaziz City for Science and Technology.
- Kampes, B. M. (2006). *Radar interferometry: Persistent Scatterer technique, remote sensing and digital image processing 12*. Springer.
- Kellogg, K. S., & Reynolds, R. L. (1983). Opening of the Red Sea: Constraints from a palaeomagnetic study of the as Sarat volcanic field, South-Western Saudi Arabia. *Geophysical Journal International*, 74, 649–665.
- Khan, A., Khan, S., & Kakar, D. (2013). Land subsidence and declining water resources in Quetta Valley, Pakistan. *Environmental Earth Sciences*, 70, 2719–2727.
- Konert, G., Afifi, A. M., Al-Hajri, S., et al. (2001). Paleozoic stratigraphy and hydrocarbon habitat of the Arabian plate. *GeoArabia*, 6(3), 407–442.
- Lloyd, J., & Pim, R. (1990). The hydrogeology and groundwater resources development of the Cambro-Ordovician sandstone aquifer in Saudi Arabia and Jordan. *Journal of Hydrology*, 121, 1–20.
- Maliva, R., & Missimer, T. (2012). *Compaction and land subsidence. Arid lands water evaluation and Management* (pp. 343–363). Springer.
- Margat, J. (2007). *Great aquifer systems of the world. Aquifer systems management: Darcy's legacy in a world of impending water shortage* (pp. 105–116).
- Martínez, P. J., Marín, M., Burbey, T. J., et al. (2013). Land subsidence and ground failure associated to groundwater exploitation in the Aguascalientes Valley, Mexico. *Engineering Geology*, 164, 172–186.
- McGillivray, J. G., & Husseni, M. I. (1992). The Paleozoic petroleum geology of Central Arabia. *American Association of Petroleum Geologists Bulletin*, 76, 1473–1490.
- MOAW (Ministry of Agriculture and Water). (1984). *Agriculture statistical yearbook*. Department of Economic Studies and Statistics.
- MOAW (Ministry of Agriculture and Water). (2004). *Agriculture statistical yearbook*. Department of Economic Studies and Statistics.
- Mohamed, A., Sultan, M., Ahmed, M., et al. (2017). Aquifer recharge, depletion, and connectivity: Inferences from GRACE, land surface models, and geochemical and geophysical data. *Geological Society of America Bulletin*, 129, 534–546.
- Morsy, E. A., & Othman, A. (2020). Assessing the impact of groundwater mixing and sea water intrusion on oil production in coastal oil fields using resistivity sounding methods. *Arabian Journal of Geosciences*, 13, 434. <https://doi.org/10.1007/s12517-020-05469-6>
- Motagh, M., Djamour, Y., Walter, T., Wetzel, H., Zschau, J., & Arabi, S. (2007). Land subsidence in Mashhad Valley, Northeast Iran: Results from InSAR, levelling and GPS. *Geophysical Journal International*, 168, 518–526.
- Motagh, M., Walter, T. R., Sharifi, M. A., Fielding, E., Schenk, A., Anderssohn, J., & Zschau, J. (2008). Land subsidence in Iran caused by widespread water reservoir overexploitation. *Geophysical Research Letters*, 35(16), L16403.
- Othman, A., & Abotalib, A. Z. (2019). Land subsidence triggered by groundwater withdrawal under hyper-arid conditions: Case study from Central Saudi Arabia. *Environmental Earth Sciences*, 78(7), 243.
- Othman, A., Sultan, M., Becker, R., et al. (2018). Use of geophysical and remote sensing data for assessment of aquifer depletion and related land deformation. *Surveys in Geophysics*, 39, 543–566. <https://doi.org/10.1007/s10712-017-9458-7>
- Poland, J. (1960). Land subsidence in the San Joaquin Valley, California, and its effect on estimates of ground-water resources. *International Association of Hydrological Sciences*, 52, 324–335.
- Powers, R., Ramirez, L., Redmond, C., & Elberg, E. (1966). *Geology of the Arabian peninsula: Sedimentary geology of Saudi Arabia*. U. S. Geological Survey. Professional Paper: a review of the sedimentary geology of Saudi Arabia, Alexandria, Virginia 560:1–147.

- Rateb, A., & Abotalib, A. Z. (2020). Inferencing the land subsidence in the Nile Delta using Sentinel-1 satellites and GPS between 2015 and 2019. *Science of the Total Environment*, 729, 138868.
- Ren, G., Whittaker, B., & Reddish, D. (1989). Mining subsidence and displacement prediction using influence function methods for steep seams. *International Journal of Mining Science and Technology*, 8, 235–251.
- Rodell, M., Houser, P., Jambor, U., et al. (2004). The global land data assimilation system. *Bulletin of the American Meteorological Society*, 85, 381–394.
- Roobol, M., Shouman, S., & Al-Solami, D. (1985). *Earth tremors, ground fractures, and damage to buildings at Tabah*. Saudi Arabian Deputy Ministry for Mineral Resources Technical Record, DGMR–TR-05-4.
- Rouse, Jr J, Haas, R, Schell, J, & Deering, D. (1974). *Monitoring vegetation systems in the Great Plains with ERTS*, NASA. Goddard Space Flight Center 3d ERTS-1 Symp 1, Sect A, pp. 309–317.
- Save, H., Bettadpur, S., & Tapley, B. D. (2016). High-resolution CSR GRACE RL05 mascons. *Journal of Geophysical Research: Solid Earth*, 121, 7547–7569.
- Scanlon, B. R., Zhang, Z., Save, H., et al. (2016). Global evaluation of new GRACE mascon products for hydrologic applications. *Water Resources Research*, 52, 9412–9429.
- Scharroo, R., & Visser, P. (1998). Precise orbit determination and gravity field improvement for the ERS satellites J Geophys res. *Oceans*, 103, 8113–8127.
- Strassberg, G., Scanlon, B. R., & Rodell, M. (2007). Comparison of seasonal terrestrial water storage variations from GRACE with groundwater-level measurements from the high plains aquifer (USA). *Geophysical Research Letters*, 34(14), L14402.
- Sultan, M., Sturchio, N., Al Sefry, S., et al. (2008). Geochemical, isotopic, and remote sensing constraints on the origin and evolution of the Rub Al Khali aquifer system, Arabian Peninsula. *Journal of Hydrology*, 356, 70–83.
- Sultan, M., Yousef, A., Metwally, S., et al. (2011). Red Sea rifting controls on aquifer distribution: Constraints from geochemical, geophysical, and remote sensing data. *Geological Society of America Bulletin*, 123, 911–924.
- Sultan, M., Ahmed, M., Wahr, J., Yan, E., & Emil, M. K. (2014). *Monitoring aquifer depletion from space: Case studies from the Saharan and Arabian aquifers. Remote sensing of the terrestrial water cycle* (pp. 347–366). Wiley.
- Sultan, M., Sturchio, N. C., Alsefry, S., Emil, M. K., Ahmed, M., Abdelmohsen, K., AbuAbdullah, M. M., Yan, E., Save, H., Alharbi, T., Othman, A., & Chouinard, K. (2019). Assessment of age, origin, and sustainability of fossil aquifers: A geochemical and remote sensing–based approach. *Journal of Hydrology*. <https://doi.org/10.1016/j.jhydrol.2019.06.017>
- Tapley, B. D., Bettadpur, S., Watkins, M., & Reigber, C. (2004). The gravity recovery and climate experiment: Mission overview and early results. *Geophysical Research Letters*, 31(9).
- Taylor, R. G., Scanlon, B., Döll, P., et al. (2013). Ground water and climate change. *Nature Climate Change*, 3, 322–329.
- Vincent, P. (2008). *Environmental impacts and hazards, Saudi Arabia: An environmental overview* (pp. 216–245). Taylor & Francis.
- Wagner, W. (2011). The Arabian plate: Geology and Hydrogeologic characteristics (Chapter 1). In *Groundwater in the Arab Middle East* (pp. 1–54). Springer.
- Wallace, C., Dinin, S., & Al-Farasani, A. (2000). *Geologic map of the Wadi as-Sirhan quadrangle, sheet 30C*. Kingdom of Saudi Arabia, Saudi Geological Survey.
- Wouters, B., Bonin, J., Chambers, D., et al. (2014). GRACE, time-varying gravity, earth system dynamics and climate change. *Reports on Progress in Physics*, 77, 116801.
- Youssef, A. M., Sabtan, A. A., Maerz, N. H., & Zabramawi, Y. A. (2014). Earth fissures in Wadi Najran. Kingdom of Saudi Arabia. *Natural Hazards*, 71, 2013–2027.
- Youssef, A. M., Al-Harbi, H. M., Gutiérrez, F., et al. (2016). Natural and human-induced sinkhole hazards in Saudi Arabia: Distribution, investigation, causes and impacts. *Hydrogeology Journal*, 24, 625–644.